


Extracellular Vesicles Derived from Wharton's Jelly Mesenchymal Stem Cells Prevent and Resolve Programmed Cell Death Mediated by Perinatal Hypoxia-Ischemia in Neuronal Cells

Marianne S. Joerger-Messerli^{1,2}, Byron Oppliger^{1,2},
 Marialuigia Spinelli^{1,2}, Gierin Thomi^{1,2,3}, Ivana di Salvo^{1,2},
 Philipp Schneider^{1,2}, and Andreina Schoeberlein^{1,2}

Cell Transplantation
 2018, Vol. 27(1) 168–180
 © The Author(s) 2018
 Reprints and permission:
sagepub.com/journalsPermissions.nav
 DOI: 10.1177/0963689717738256
journals.sagepub.com/home/ctt


Abstract

Hypoxic-ischemic (HI) insult in the perinatal phase harbors a high risk of encephalopathy in the neonate. Brain cells undergo apoptosis, initiating neurodegeneration. So far, therapeutic approaches such as cooling remain limited. Transplantation of mesenchymal stem cells (MSCs) exhibits therapeutic success despite the short-time survival in the host brain, providing strong evidence that their beneficial effects are largely based on secreted factors, including extracellular vesicles (EVs). The aim of this study was to investigate the effects of human Wharton's jelly MSC (hWJ-MSC)-derived EVs on neuroprotection and neuroregeneration, using an in vitro model of oxygen–glucose deprivation/reoxygenation (OGD/R) mimicking HI injury in the mouse neuroblastoma cell line neuro2a (N2a). hWJ-MSC-derived EVs were isolated from cell culture supernatants by multistep centrifugation and identified by endosomal marker expression and electron microscopy. OGD/R significantly increased DNA fragmentation and *caspase 3* (*Casp3*) transcription in N2a cells relative to undamaged cells. OGD/R-mediated DNA fragmentation and *Casp3* expression could be prevented as well as resolved by the addition of hWJ-MSC-derived EV before and after OGD, respectively. hWJ-MSC-derived EV also tended to increase the phosphorylation of the B cell lymphoma 2 (Bcl2) family member Bcl-2-antagonist of cell death (BAD) in N2a cells, when added prior or post OGD, thereby inactivating the proapoptotic function of BAD. Fluorescence confocal microscopy revealed the close localization of hWJ-MSC-derived EVs to the nuclei of N2a cells. Furthermore, EVs released their RNA content into the cells. The expression levels of the microRNAs (miRs) let-7a and let-7e, known regulators of *Casp3*, were inversely correlated to *Casp3*. Our data suggest that hWJ-MSC-derived EVs have the potential to prevent and resolve HI-induced apoptosis in neuronal cells in the immature neonatal brain. Their antiapoptotic effect seems to be mediated by the transfer of EV-derived let-7-5p miR.

Keywords

extracellular vesicles (EVs), oxygen–glucose deprivation/reoxygenation (OGD/R), apoptosis, neuroprotection, neuroregeneration, let-7-5p

Introduction

The human brain has a great demand for oxygen and glucose, which are used in oxidative phosphorylation to generate adenosine triphosphate (ATP), providing chemical energy to the cell. Hypoxia-ischemia (HI) leads to the rapid reduction in oxidative phosphorylation and, subsequently, to primary energy failure in glutamatergic neuronal cells¹. HI in the perinatal phase reduces the ATP availability and frequently leads to brain injury implying inflammation and cell death. In contrast to the adult brain, the prominent kind of

¹ Department of Obstetrics and Gynecology, Bern University Hospital (Inselspital), University of Bern, Bern, Switzerland

² Department of BioMedical Research, University of Bern, Bern, Switzerland

³ Graduate School for Cellular and Biomedical Sciences (GCB), University of Bern, Bern, Switzerland

Submitted: March 01, 2017. Revised: September 27, 2017. Accepted: September 28, 2017.

Corresponding Author:

Andreina Schoeberlein, Laboratory for Prenatal Medicine, Department of BioMedical Research, KiKI E838, Inselspital, 3010 Bern, Switzerland.
 Email: andreina.schoeberlein@dbmr.unibe.ch



Creative Commons CC BY-NC: This article is distributed under the terms of the Creative Commons Attribution-NonCommercial 4.0 License (<http://www.creativecommons.org/licenses/by-nc/4.0/>) which permits non-commercial use, reproduction and distribution of the work without further permission provided the original work is attributed as specified on the SAGE and Open Access pages (<https://us.sagepub.com/en-us/nam/open-access-at-sage>).

cell death in the neonatal brain after HI is the highly regulated programmed cell death, namely, apoptosis^{2,3}. Caspase-dependent death pathways are activated in many brain cell types, initiating neurodegeneration⁴⁻⁶. Severe lifelong neurodevelopmental manifestations, such as motor deficits including cerebral palsy, can be a consequence. Together with the severity of the HI insult, the maturity degree of the brain determines the severity of HI brain damage, thus, increasing the risk of encephalopathy in preterm neonates⁷. To date, hypothermia is the only therapeutic intervention used clinically for infants with HI brain damage born at term or late preterm (≥ 35 wk of gestation). Although it lowers infant mortality and morbidity, therapeutic hypothermia does not guarantee complete protection^{8,9}. Because of the lack of an effective therapy for premature infants, supportive care is the only available treatment option after preterm HI brain damage. Hence, there is an immediate need for selective therapeutic agents.

We and others have shown that the transplantation of mesenchymal stem cells (MSCs) has neuroregenerative potential in animal models of perinatal HI brain injury.¹⁰⁻¹² As transplanted MSCs have beneficial effects in spite of low long-ranging survival in host tissue¹³, the therapeutic impact of applied MSCs largely relies on released factors, including extracellular vesicles (EVs)^{14,15}. When EVs were discovered over 30 y ago^{16,17}, they were considered a by-product of the cells without specific functions. However, since Raposo et al. revealed the intercellular communication potential of EVs in 1996¹⁸, and the significance of the intercellular transport of proteins, lipids, and nucleic acids by EVs has been emphasized by numerous publications¹⁹. EVs can be classified into apoptotic bodies, microvesicles (MVs), and exosomes. MVs and exosomes both contain nucleic acids, lipids, and cytoplasmic and membrane proteins. However, they differ in size and biogenesis. While MVs have a diameter of 50 to 1,000 nm and are shed directly from the plasma membrane, exosomes have a diameter of 30 to 120 nm and originate from the endosomal membrane²⁰. The exact differences between MVs and exosomes has been shown to be complex and led to confusion among scientists. Thus, we will use EVs as an umbrella term, as recommended by the International Society of Extracellular Vesicles. In 2011, Zhuang et al. successfully transplanted EVs intranasally in mouse models of brain inflammatory diseases²¹. EVs reached the brain within 30 min²¹. Furthermore, MSC-derived EVs have been shown to exhibit neuroregenerative potential in rodent stroke models by inducing neurite outgrowth²², reducing motor coordination deficits, and increasing angiogenesis^{23,24}. In an ovine model of preterm HI brain injury, Ophelders et al. recently demonstrated that the in utero intravenous administration of bone marrow-derived MSC (BM-MSC)-EVs after global HI decreased the number and duration of seizures and tended to obviate hypomyelination²⁵. These observations make EVs a promising alternative to MSCs to treat perinatal HI brain injury. Furthermore, therapeutic intervention with EVs provides huge advantages over

cell-based therapy²⁶⁻²⁸. EVs are not viable, making them safer for storage at -20°C without the addition of cryoprotectant solutions. They are less immunogenic than the mother cell, and the applied dose and biological activity can be more easily standardized. Furthermore, EVs are stable in bodily fluids and their contents are naturally protected from degradation, making them more advantageous over soluble molecules. For example, free RNA is rapidly degraded.

To date, the molecular mechanisms of the therapeutic effects of EVs are not fully understood. EVs contain a lot of bioactive molecules, which could be transferred to target cells. In addition to proteins, lipids, DNA, and mRNA, small noncoding microRNA (miR) play a key role in gene regulation and have been detected in EVs²⁹. Thus, most studies analyzing MSC-derived EVs showed that miR originating from EVs influenced the fate of target cells. In 2012, Xin et al. documented that the increased neurite outgrowth of neural cells in a rat model of middle cerebral artery occlusion (MCAO) after transplantation of BM-MSCs relied on the transfer of miR-133b by BM-MSC-derived EVs into host neural cells²². Furthermore, in a rat model of primary brain tumor, the injection of EVs derived from miR-146 expressing MSCs into gliomas significantly reduced glioma growth³⁰. The observation that MSC-derived EVs are able to reprogram tumor cells by the transfer of miR has become substantiated by Lee and coworkers³¹. They showed that EV-derived miR-16, which is known to target *VEGF*, was in part accountable for the antiangiogenic effect in breast cancer cells.

Thus, in the present study, we evaluate the neuroprotective and neuroregenerative effects of human Wharton's jelly MSC (hWJ-MSC)-derived EVs on neuroblastoma cells in an in vitro model of HI damage.

Materials and Methods

Isolation and Culture of Human Wharton's Jelly-derived Mesenchymal Stem Cells (hWJ-MSCs)

Following cesarean section, umbilical cords from healthy term deliveries (mean gestational age 38.9 (0.6) wk [standard deviation]; $n = 5$) were collected after informed consent. The institutional review board of the University Hospital Bern and the Canton of Bern approved the study. hWJ-MSCs were isolated as described previously³² and cultured in Dulbecco's modified Eagle's medium (DMEM)/F12 supplemented with 10% fetal calf serum (FCS), 2 mmol/L glutamax, and 100 units/mL penicillin/100 $\mu\text{g}/\text{mL}$ streptomycin (expansion medium; Thermo Fisher Scientific, Waltham, MA, USA).

Isolation of hWJ-MSC-derived EVs

hWJ-MSC-derived EVs were isolated by serial centrifugations as described by Théry et al.³³ In brief, as hWJ-MSCs reached 70% to 80% confluency, the cells were washed twice with phosphate-buffered saline (PBS). The expansion

medium was replaced by serum-free DMEM/F12 containing 2 mmol/L glutamax and 100 units/mL penicillin/100 µg/mL streptomycin to avoid the contamination with EVs originating from FCS. The conditioned medium (CM) for EV purification was collected after 24 h of culture. The viability of hWJ-MSCs was assessed by trypan blue exclusion using the Countess II FL Automated Cell Counter (Thermo Fisher Scientific). To pellet the cells, CM was centrifuged at 300g for 10 min. The supernatant was centrifuged at 2,000g for 10 min to remove dead cells. To pellet cellular debris, the supernatant was centrifuged at 10,000g for 30 min. To finally obtain EVs, the supernatant was centrifuged at 100,000g for 70 min. EVs were washed with 5 mL PBS and centrifuged a second time at 100,000g for 70 min. The pelleted EVs were resuspended in PBS and stored at -20°C until use.

Quantification and Characterization of hWJ-MSC-derived EVs

The protein content of hWJ-MSC-derived EVs was measured using the NanoVue Plus™ spectrophotometer (Biochrom, Holliston, MA, USA). The isolated vesicles were examined for the expression of endosomal proteins by the Exo-Check-antibody array (System Biosciences, Palo Alto, CA, USA) and by determining their size by negative-staining electron microscopy.

Exo-Check antibody array. The semiquantitative Exo-Check antibody array is a membrane-based assay with 12 pre-printed spots comprising antibodies against the known exosomal markers CD63, CD81, apoptosis-linked gene 2-interacting protein X (ALIX), flotillin 1, intercellular adhesion molecule 1 (ICAM-1), epithelial cell adhesion molecule (EpCAM), annexin A5 (ANXA5), and tumor susceptibility gene 101 (TSG101). The GM130 cis-Golgi protein marker acts as negative control to rule out cellular contamination. The positive control contains human serum exosome proteins. The Exo-Check antibody array was performed according to the manufacturer's protocol. Detection was done by chemiluminescence using Amersham ECL Prime Western blotting reagent (GE Healthcare Life Sciences, Piscataway, NJ, USA) on a Chemidoc XRS+ system from Bio-Rad Laboratories, Inc. (Hercules, CA, USA).

Negative-staining electron microscopy. For the imaging of negatively stained samples, aliquots of 5 µL hWJ-MSC-derived EVs were adsorbed on Formvar® (Formvar resin 15/95, Ted Pella, Inc., Redding, CA, USA) coated copper grids, washed 3 times with pure water, and stained with 2% uranyl acetate solution (Electron Microscopy Sciences, Hatfield, PA, USA) for 30 s. Excess fluid was removed by gently pushing them sideways to filter paper. Samples were examined with a transmission electron microscope (CM12, Philips, Eindhoven, the Netherlands), equipped with a digital camera (MORADA, Soft Imaging System, Münster, Germany) and image analysis software (iTEM; OSIS, Olympus Soft Imaging

Solutions, Münster, Germany). The mean EV diameter was calculated using the ImageJ software (NIH, Bethesda, MD, USA). To get pixels per nanometer, the length in pixels of the scale bar was calculated with the tool "straight." The scale bar and truncated EVs at the border of the image were cleared to exclude them from the analysis. Then, the image was inverted and the threshold was adjusted using "auto-threshold." The EVs were analyzed for the parameters "area" and "perimeter" using the following filter mask settings: size (pixels²) = 1,000–1,5000; circularity = 0.11–1.00. The obtained pixels were converted to nanometer, and the average diameter of the EVs was calculated from the area and perimeter.

GRP94 Western Blotting of EVs

Twenty microliters of WJ-MSCs, lysed using the mammalian cell lysis kit from Sigma-Aldrich (St. Louis, MO, USA), and EV were separated by sodium dodecyl sulfate–polyacrylamide gel electrophoresis (SDS-PAGE) on a 4% to 20% gradient gel (Bio-Rad) to analyze the expression of the chaperone GRP94. Separated proteins were transferred onto nitrocellulose membranes (Thermo Fisher Scientific), blocked with 5% milk, and analyzed with a rabbit antibody against GRP94 (1:500; Cell Signalling Technology, Danvers, MA, USA). As secondary antibody, horseradish peroxidase (HRP)-coupled donkey anti-rabbit (1:1,000; GE Healthcare Life Sciences) was used. Binding was detected by chemiluminescence using Amersham ECL Prime Western blotting reagent (GE Healthcare Life Sciences) on a Chemidoc XRS+ system Bio-Rad.

Culture of Mouse Neuroblastoma Cell Line Neuro2a (N2a)

The mouse neuroblastoma cell line N2a was purchased from American Type Culture Collection (ATCC, Manassas, VA, USA) and expanded in DMEM containing 10% FCS, 2 mmol/L glutamax, and 100 units/mL penicillin/100 mg/mL streptomycin (N2a expansion medium). Trypsin-ethylenediaminetetraacetic acid (EDTA, 0.25%; Thermo Fisher Scientific) was used to detach N2a cells from culture plates.

Oxygen–Glucose Deprivation and Reoxygenation (OGD/R)

N2a cells were seeded at 9,000 cells/cm² and cultured overnight in N2a expansion medium. The next day, the N2a expansion medium was replaced by glucose-free DMEM, supplemented with 10% FCS, 2 mmol/L glutamax, and 100 units/mL penicillin/100 mg/mL streptomycin, and incubated for 6 h at 37 °C in 1% O₂/5% CO₂ (hypoxia). After OGD, medium was replaced by N2a expansion medium and returned into a normoxic incubator for 24 h or 48 h and subsequently analyzed for cellular damage.

To assess the protective and therapeutic effects of hWJ-MSC-derived EVs, 0.1 µg/mL (2.02 pg/cell) or 1 µg/mL EVs (20.2 pg/cell) were added either 24 h or 1 h before OGD induction or directly after the 6 h of OGD. N2a cells were analyzed after 24 h and 48 h of reoxygenation.

Terminal Deoxynucleotidyl Transferase deoxyuridine triphosphate Nick End Labeling (TUNEL) Test

The In Situ Cell Death Detection Kit (Sigma-Aldrich) was used to detect and quantify apoptosis based on the labeling of DNA strand breaks. The cells were fixed with 4% paraformaldehyde (PFA) in PBS, pH 7.4 for 1 h at room temperature. Fixed cells were washed with PBS and permeabilized with 0.1% Triton X-100 in 0.1% sodium citrate for 2 min on ice. Cells were washed twice with PBS and stained with the TUNEL reaction mixture in a humidified atmosphere at 37 °C for 1 h according to the manufacturer's protocol. Nuclei were counterstained with 4'-6-diamidino-2-phenylindole-dihydrochloride (DAPI, Sigma-Aldrich). Stained cells were washed 3 times with PBS and analyzed with a DM IL microscope (Leica Microsystems, Wetzlar, Germany).

RNA Extraction from N2a cells, Reverse Transcription, and Real-time Polymerase Chain Reaction (PCR)

RNA was extracted using the QIAshredder and the Allprep DNA/RNA/Protein Mini Kits (Qiagen, Hilden, Germany), according to the manufacturer's protocol. The concentration of RNA was assessed by a NanoVue Plus™ spectrophotometer (Biochrom).

Up to 5 µg of total RNA were reverse transcribed by the SuperScript III First-Strand Synthesis System (Thermo Fisher Scientific). The transcription of *caspase 3* (*Casp3*, GE assay ID: Mm01195085_m1; Thermo Fisher Scientific) and B-Cell CLL/lymphoma 2-associated agonist of cell death (*Bad*, GE assay ID: Rn00575519_m1; Thermo Fisher Scientific) was assessed by real-time PCR. The following PCR cycling program was run on a 7300 Real-Time PCR System (Thermo Fisher Scientific): 2 min at 50 °C, 10 min at 95 °C, followed by 45 cycles of 15 s at 95 °C and 1 min at 60 °C. The transcripts were normalized to the reference gene glyceraldehyde-3-phosphate dehydrogenase (*Gapdh*) and analyzed using the 7300 System Software (Thermo Fisher Scientific). Data were expressed as fold change relative to untreated N2a cells.

For the reverse transcription of miR, the miScript II RT kit (Qiagen) was used. According to the manufacturer's protocol, 125 to 250 ng of total RNA were needed per reaction. The expression levels of let-7a (cat.no. MS00006482, Qiagen) and let-7e (cat. no. MS00031227, Qiagen) were measured by SYBR Green-based real-time PCR. The following PCR cycling program was used: 15 min at 95 °C, followed by 45 cycles of 15 s at 94 °C, 30 s at 55 °C, and 34 s at 70 °C. Let-7a and let-7e levels were normalized to snord95

(cat. no. MS00033726, Qiagen) and analyzed using the 7300 System Software. Data were expressed as fold change relative to untreated N2a cells.

RNA Extraction from EV, Reverse Transcription, and Real-time PCR of miR

EV RNA was extracted using the Total Exosome RNA and Protein Isolation kit (Thermo Fisher Scientific). miR was reverse transcribed using the miScript II RT kit (Qiagen). The human Neurological Development and Disease miScript™ miRNA PCR Array (Cat. No. MIHS-107Z; Qiagen) is an SYBR Green-based real-time PCR array and was used to profile the presence of mature miR involved in neurological development and progression of neurological diseases in EVs. For one 96-well plate, 100 µL of cDNA, which was pooled equally from 4 different EV preparations, were mixed with 1,375 µL of 2× QuantiTect SYBR Green PCR Master Mix (Cat.No. 218073) and 275 µL of 10× miScript Universal Primer and filled up with RNase-free water to the final volume of 2,750 µL. Twenty-five microliters of the PCR component mix were pipetted into each well of the PCR array. The PCR was run with the following PCR cycling program on a 7300 Real-Time PCR System (Thermo Fisher Scientific): 15 min at 95 °C, followed by 45 cycles of 15 s at 94 °C, 30 s at 55 °C, and 34 s at 70 °C.

The online database miRDB.org was used for miR target gene prediction. Using a computational target prediction algorithm, the program calculates the probability of the binding of the miR to a certain gene, which yields a target score between 50 and 100. The higher the target score is, the more likely is the binding.

Protein Isolation and p-BAD Serine at Position 112 (Ser112) Western Blotting

Protein was isolated using the QIAshredder and the Allprep DNA/RNA/Protein Mini Kits (Qiagen) according to the manufacturer's protocol. Total protein concentration was measured by the bicinchoninic acid protein assay kit (Sigma-Aldrich).

Proteins were separated by SDS-PAGE on a 15% gel for the analysis of the phosphorylation of BAD at the Ser112 site (p-BADSer112). Separated proteins were transferred onto nitrocellulose membranes (Thermo Fisher Scientific), blocked with 5% bovine serum albumin (BSA) and analyzed with a rabbit antibody against p-BADSer112 (1:500; Cell Signalling Technology). HRP-coupled donkey anti-rabbit (1:1,000; GE Healthcare Life Sciences) was used as secondary antibody. Binding was detected by chemiluminescence using Amersham ECL Prime Western blotting reagent (GE Healthcare Life Sciences) on a Chemidoc XRS+ system from Bio-Rad Laboratories GmbH.

ImageJ software was used for pixel summation of individual bands. Pixel intensities were corrected for background.

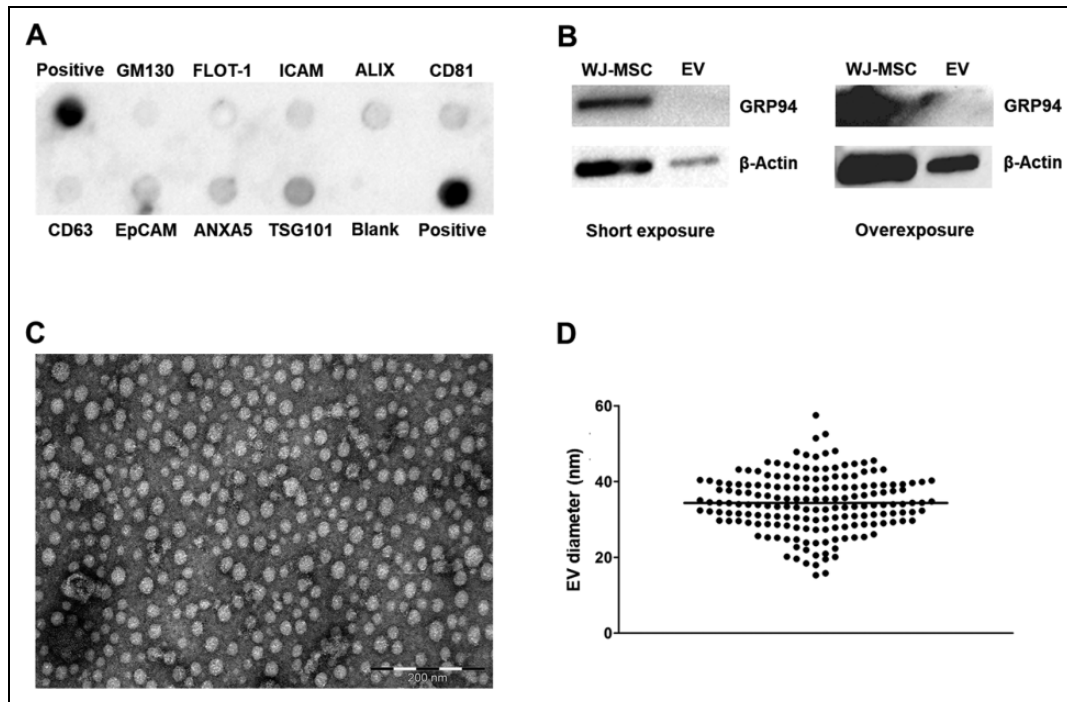


Fig. 1. Characterization of human Wharton's jelly mesenchymal stem cells (hWJ-MSC)-derived extracellular vesicles (EVs). (A) Representative Exo-Check antibody array of isolated hWJ-MSC-derived EVs. The antibody array has been done with 4 different EV preparations. (B) Western blot analysis of GRP94 expression in hWJ-MSC lysates and hWJ-MSC-derived EVs. Anti- β -actin staining was used as loading control, even though it is more abundant in cells than in EVs. To prove absent GRP94 expression in EVs, the membrane was overexposed. Western blot analysis has been done for 3 different EV preparations. (C) Representative electron microscopy image of hWJ-MSC-derived EVs, (D) revealing a mean vesicle diameter of 34.34 nm. Electron microscopy has been performed with 2 different EV preparations.

p-BADSer112 intensities were standardized to the corresponding β -actin bands.

Culture of N2a Cells with Chloromethyl (CM)-Dil- and Exo-Red-labeled hWJ-MSC-derived EVs

EVs were stained with 2 μ M of the fluorescent celltracker™ dye CM-Dil (Thermo Fisher Scientific) according to the manufacturer's protocol. CM-Dil-stained EVs were centrifuged for 70 min at 100,000g at 4 °C and resuspended in PBS. 37,500 N2a cells/cm² were cultured with 5 μ g/mL CM-Dil-stained EVs for 24 h. Nuclei were counterstained with DAPI (Sigma-Aldrich). Optical sections were taken using a Zeiss LSM 710 (Carl Zeiss AG, Feldbach, Switzerland), with a 63 \times oil objective (Plan-Apochromat 63 \times /1.40 Oil DIC M27) and a digital zoom of 1.0.

EV RNA was labeled with the red fluorescent Exo-Red (Exo Glow™ Exosome labeling kit, System Biosciences) according to the manufacturer's protocol. Exo-Red-stained EVs were cultured for 2 h with 37,500 N2a cells/cm². Nuclei were counterstained with DAPI (Sigma-Aldrich). Analysis was done on a DM6000 B microscope (Leica Microsystems).

Statistical Analysis

Statistical analysis was done using the SigmaPlot software version 11.0 (Systat Software, Inc., Chicago, IL, USA). To

calculate the significance of real-time PCR data, one-way repeated measures analysis of variance (ANOVA) was performed, followed by the all pairwise multiple comparison Holm-Sidak test in case of a significant effect. *t*-tests were used for the statistical analysis of the TUNEL data. All experimental groups were compared to the OGD/R group. *P* < 0.05 was considered statistically significant.

Results

Characterization of hWJ-MSC-derived EVs

The viability of hWJ-MSCs after 24 h culture in serum-free medium was $91.08 \pm 3.79\%$, as assessed by trypan blue exclusion. Over this period of time, $6.14 \mu\text{g} \pm 3.48$ EVs, quantified by their protein content, were released by 10^6 hWJ-MSCs. To assess whether the isolated hWJ-MSC-derived vesicles were of endosomal origin, they were analyzed for the expression of endosomal proteins, the absence of GM130, a cis-Golgi protein marker, and GRP94, which is the most abundant chaperone protein in the endoplasmic reticulum lumen, and for their size by negative-staining electron microscopy (Fig. 1A to D). hWJ-MSC-derived vesicles were positive for endosome-specific proteins, such as TSG101, ANXA5, tetraspanin CD81, and ALIX (Fig. 1A). Additionally, EVs were negative for GM130 and GRP94, ruling out the presence of organelle fractions, such as Golgi

apparatus and endoplasmic reticulum, a hallmark of apoptotic bodies, in the isolated EVs (Fig. 1A and B).

Electron microscopy revealed that the EVs were similar in size and had a roundish morphology (Fig. 1C). The mean diameter of the EVs in Fig. 1C was determined (Fig. 1D). The calculation of the length of the 200 nm scale bar yielded 812 pixels, assuming that 1 nm corresponds to 4.06 pixels. The calculated diameters in pixels were converted into nanometer, resulting in a mean EV diameter of 34.34 nm.

hWJ-MSC-derived EVs Prevent OGD/R-triggered Apoptosis in N2a Cells

To evaluate the neuroprotective potential of EVs generated from hWJ-MSCs on neural cells after an HI insult, we established an OGD/R in vitro model. As the mouse neuroblastoma cell line N2a has been previously used to study neuroprotection in vitro³⁴, we subjected N2a cells to 6 h of OGD, followed by 24 h and 48 h of reoxygenation, respectively. hWJ-MSC-derived EVs were added 24 h or 1 h before the onset of OGD (Fig. 2A).

Six hours of OGD and 24 h of reoxygenation significantly increased the percentage of TUNEL-positive cells relative to the undamaged N2a cells ($P = 0.0057$; Fig. 2E). The addition of 0.1 $\mu\text{g}/\text{mL}$ (ca. 2 pg/cell; $P = 0.003$) or 1 $\mu\text{g}/\text{mL}$ (ca. 20 pg/cell; $P = 0.004$) EVs to N2a cells 1 h before the initiation of OGD prevented the increase of OGD/R-mediated TUNEL expression (Fig. 2E).

Given that *Casp3* activation plays a key role in the HI damage of immature brain^{35–37}, we assessed *Casp3* expression in N2a cells subjected to OGD/R. In response to 6 h of OGD and 48 h of reoxygenation, *Casp3* levels were significantly upregulated ($P = 0.002$), which was prevented by the addition of 0.1 $\mu\text{g}/\text{mL}$ (ca. 2 pg/cell; $P = 0.024$) and 1 $\mu\text{g}/\text{mL}$ (ca. 20 pg/cell; $P = 0.048$) EV 24 h and 0.1 $\mu\text{g}/\text{mL}$ (ca. 2 pg/cell; $P = 0.024$) EV 1 h before OGD exposure (Fig. 2F). Six hours of OGD followed by 24 h of reoxygenation did not alter *Casp3* transcription in N2a cells compared to control cells (data not shown).

A further key player during apoptosis is the proapoptotic Bcl-2 family member BAD³⁸. The transcription of *Bad* was significantly increased in N2a cells relative to undamaged N2a cells in response to 6 h of OGD and 48 h of reoxygenation ($P = 0.024$; Fig. 2G). The addition of 0.1 $\mu\text{g}/\text{mL}$ (ca. 2 pg/cell) and 1 $\mu\text{g}/\text{mL}$ (ca. 20 pg/cell) EV 24 h and 1 h before OGD/R, however, did not significantly increase *Bad* (Fig. 2G). At the protein level, the proapoptotic activity of BAD is regulated by phosphorylation. Phosphorylated BAD (p-BAD) is restrained in the cytosol. The dephosphorylation of BAD results in the translocation to mitochondria promoting the release of cytochrome C. BAD contains 3 phosphorylation sites. Here, we studied the phosphorylation of Ser112 (p-BADSer112) by Western blotting. Six hours of OGD and the reoxygenation of 24 h and 48 h, respectively, did not alter the expression of p-BADSer112 (Figs. 2H and 3G). In contrast, the addition of 0.1 $\mu\text{g}/\text{mL}$ and 1 $\mu\text{g}/\text{mL}$ EVs

24 h and 1 h before OGD, followed by 24 h or 48 h of reoxygenation, respectively, enhanced the level of p-BADSer112 by trend (Fig. 2H).

hWJ-MSC-derived EVs Resolve OGD/R-triggered Apoptosis in N2a Cells

From a clinical point of view, the neuroregenerative effects of EVs are more relevant than the neuroprotective ones. Thus, we investigated the potential curative effects of hWJ-MSC-derived EVs on OGD/R subjected N2a cells. EVs were added immediately after OGD (Fig. 3A). The treatment of N2a cells with 1 $\mu\text{g}/\text{mL}$ (ca. 20 pg/cell) hWJ-MSC-derived EVs after OGD and 24 h of reoxygenation resolved the rise of TUNEL-positive cells caused by OGD/R ($P = 0.02$; Fig. 3E).

Furthermore, the treatment with both 0.1 $\mu\text{g}/\text{mL}$ (ca. 2 pg/cell; $P = 0.024$) or 1 $\mu\text{g}/\text{mL}$ (ca. 20 pg/cell; $P = 0.024$) hWJ-MSC-derived EVs reversed the upregulated transcription of *Casp3* in N2a cells after 48 h of reoxygenation (Fig. 3F). However, 24 h of reoxygenation did not alter *Casp3* in N2a cells relative to control cells (data not shown). *Bad* expression was not affected by the treatment with EVs after 6 h OGD and 24 h or 48 h of reoxygenation, respectively (data not shown).

Furthermore, the treatment of N2a cells after OGD with 0.1 $\mu\text{g}/\text{mL}$ (ca. 2 pg/cell) or 1 $\mu\text{g}/\text{mL}$ (ca. 20 pg/cell) EVs, followed by 24 h or 48 h of reoxygenation, respectively, tended toward an increased phosphorylation of BAD (p-BADSer112; Fig. 3G).

hWJ-MSC-derived EVs Get Internalized by N2a Cells

As hWJ-MSC-derived EVs had neuroprotective and neuroregenerative effects on N2a cells, we next assessed how hWJ-MSC-derived EVs interacted with N2a cells. For this reason, the EVs were stained with the red fluorescent lipophilic dye CM-Dil prior to the coculture with N2a cells. Fluorescence confocal microscopy revealed colocalization of the EVs and the cells after 24 h of coculture (Fig. 4A and B). hWJ-MSC-derived EVs mostly formed aggregates and were localized close to the nuclei of N2a cells.

hWJ-MSC-derived EVs Contain miR Targeting Proapoptotic Genes and Release Their RNA Content into N2a Cells

Along with DNA, mRNA, proteins, and lipids, EV transport highly conserved, small noncoding miR molecules, which have decisive functions in gene regulation²⁹. Thus, addressing the potential molecular mechanism of neuroprotection and neuroregeneration, we next evaluated whether hWJ-MSC-derived EVs transfer their RNA into N2a cells. EV RNA was stained with the red fluorescent dye Exo-Red prior to the coculture with N2a cells. After 2 h of co-incubation,

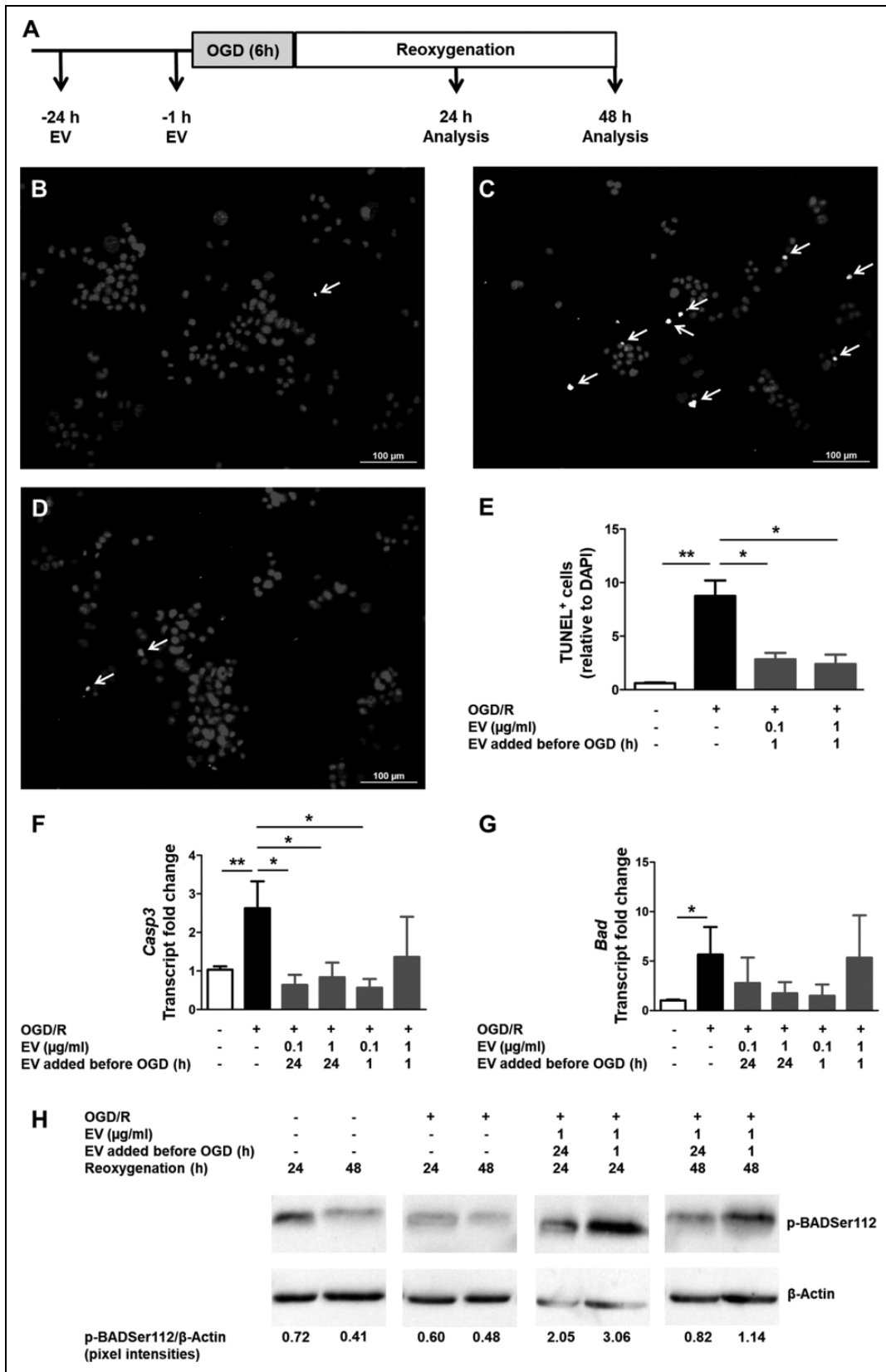


Fig. 2. Prevention of oxygen–glucose deprivation/reoxygenation (OGD/R)-triggered apoptosis in neuro2a (N2a) cells by human Wharton’s jelly mesenchymal stem cells (hWJ)-MSC-derived extracellular vesicles (EVs). N2a cells were either left undamaged or subjected to 6 h of oxygen–glucose deprivation (OGD), followed by 24 h or 48 h of reoxygenation, respectively. To test the neuroprotective capacity of hWJ-MSC-derived EVs, 0.1 μg/mL (ca. 2 pg/cell) or 1 μg/mL EVs (ca. 20 pg/cell) were added to the cells 24 h or 1 h before OGD induction.

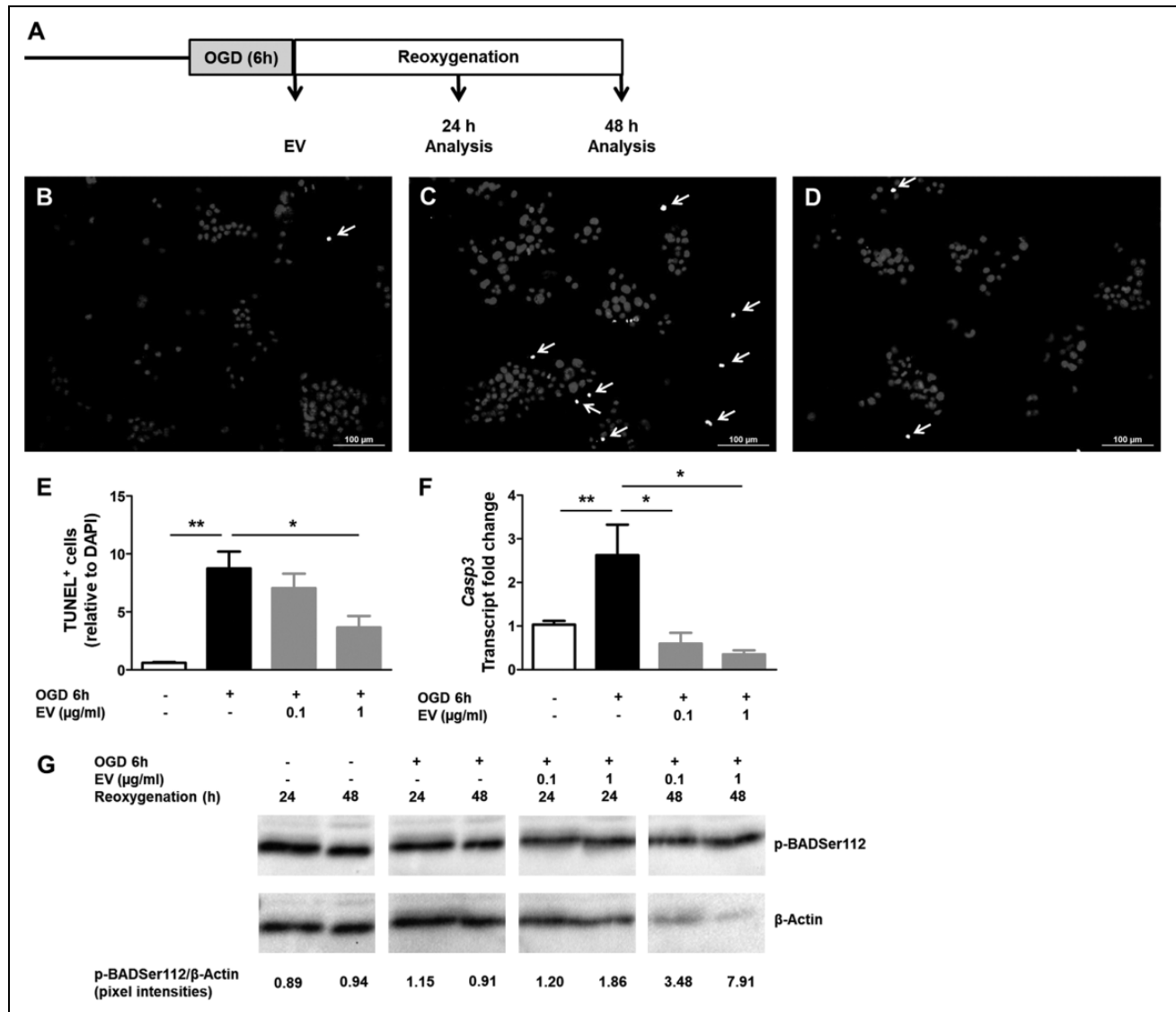


Fig. 3. Reversion of oxygen–glucose deprivation/reoxygenation (OGD/R)-triggered apoptosis in neuro2a (N2a) cells by human Wharton’s jelly mesenchymal stem cells (hWJ-MSC)-derived extracellular vesicles (EVs). N2a cells were either left undamaged or subjected to 6 h of oxygen–glucose deprivation (OGD), followed by 24 h or 48 h of reoxygenation, respectively. To test for the neuroregenerative capacity of hWJ-MSC-derived EVs, 0.1 µg/mL (ca. 2 pg/cell) or 1 µg/mL EVs (ca. 20 pg/cell) were added after 6 h of OGD. (A) Experimental outline. (B to G) After the treatment with EV post-OGD, followed by 24 h of reoxygenation, N2a cells were evaluated by terminal deoxynucleotidyl transferase dUTP nick end labeling (TUNEL) test. TUNEL-positive cells are marked by arrows. N2a nuclei were counterstained with 4’,6-diamidino-2-phenylindole (DAPI). Representative images of undamaged N2a cells (B), N2a cells subjected to OGD/R (C), and N2a cells treated with 1 µg/ml EVs after OGD (D). (E) Differences in TUNEL-positive cells relative to DAPI. Bars illustrate mean ± standard error of mean (SEM) of 6 different images. *P < 0.05, **P < 0.01. Student’s t-test. (F) Real-time polymerase chain reaction (PCR) analysis of caspase 3 transcription post 48 h of reoxygenation. Bars illustrate mean ± SEM of 3 independent experiments. *P < 0.05, **P < 0.01. Analysis of variance with post hoc Holm-Sidak test. (G) Western blot analysis for phosphorylation of BAD at the serine at position 112 site expression.

Fig. 2. (continued) (A) Experimental outline. (B to H) After the pretreatment with EVs 1 h before OGD and 24 h of reoxygenation, N2a cells were evaluated by terminal deoxynucleotidyl transferase deoxyuridine triphosphate nick end labeling (TUNEL) test. TUNEL-positive cells are marked by arrows. N2a nuclei were counterstained with 4’,6-diamidino-2-phenylindole (DAPI). Representative images of undamaged N2a cells (B), N2a cells subjected to OGD/R (C), and N2a cells pretreated with 1 µg/mL EVs before OGD initiation (D). (E) Differences in TUNEL-positive cells relative to DAPI. Bars illustrate mean ± standard error of mean (SEM) of 6 different images. *P < 0.05, **P < 0.01. Student’s t-test. (F and G) Real-time polymerase chain reaction analysis of caspase 3 and B cell lymphoma 2-associated antagonist of cell death (Bad) transcription post 48 h of reoxygenation. Bars illustrate mean ± SEM of 3 independent experiments. *P < 0.05, **P < 0.01. Analysis of variance with post hoc Holm-Sidak test. (H) Western blot analysis for phosphorylation of BAD at the serine at position 112 site expression.

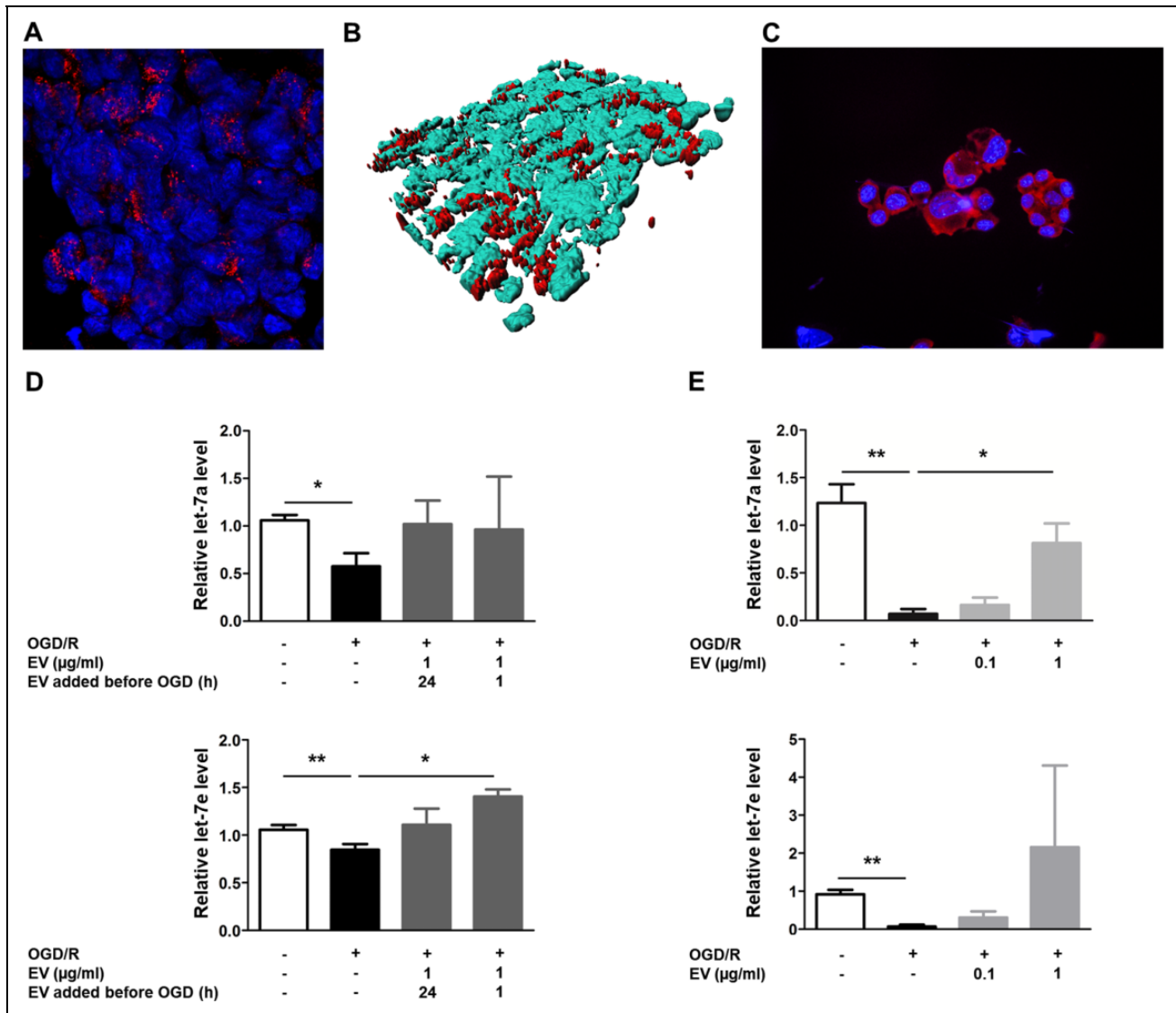


Fig. 4. Human Wharton's jelly mesenchymal stem cells (hWJ-MSC)-derived extracellular vesicles (EVs) interact with and deliver their RNA into neuro2a (N2a) cells. hWJ-MSC-derived EVs were either labeled with the membrane dye chloromethyl (CM)-Dil (red) or the RNA dye Exo-Red and cocultured with N2a cells. The nuclei of N2a cells were counterstained with 4-6-diamidino-2-phenylindole-dihydrochloride (DAPI) (blue). (A) Representative fluorescent confocal microscopy image after the coculture of CM-Dil-stained EV and N2a cells for 24 h. (B) Three-dimensional visualization of the coculture of CM-Dil-stained EV and N2a cells by fluorescent confocal microscopy. (C) Representative fluorescent microscopy image after 2 h of coculture of Exo-Red-stained EV RNA and N2a cells. (D) Real-time polymerase chain reaction (PCR) analysis of let-7a and let-7e expression in N2a cells after 6 h oxygen-glucose deprivation (OGD) and 24 h of reoxygenation with and without the pretreatment with 1 µg/mL EVs (ca. 20 pg/cell) 24 h or 1 h before OGD initiation, relative to undamaged N2a cells. (E) Real-time PCR analysis of let-7a and let-7e expression in N2a cells after 6 h OGD and 24 h of reoxygenation with and without the treatment with 1 µg/mL EVs after 6 h of OGD, relative to undamaged N2a cells. Bars illustrate mean \pm standard error of mean (SEM) of 3 independent experiments; * $P < 0.05$, ** $P < 0.01$. Analysis of variance with post hoc Holm-Sidak test.

N2a cells were highly positive for Exo-Red, confirming the delivery of EV RNA into N2a cells (Fig 4C).

Knowing that hWJ-MSC-derived EVs release their RNA into N2a cells, we were characterizing the miR content of hWJ-MSC-derived EVs by real-time PCR. Potentially relevant mature miRs targeting proapoptotic genes, being present in the isolated hWJ-MSC-EVs and their predicted target genes with a target gene ≥ 70 (according to miRDB.org), are listed in Table 1. EVs contained mature miR, which are very

likely to target and regulate the expression of numerous proapoptotic genes, including BCL2 family members, BCL2 interacting molecules, *BCL10* and *Harakiri (HRK)*, and *caspases*, in particular *Casp3*.

As shown above, hWJ-MSC-derived EVs prevented (Fig. 2E) and reversed (Fig. 3E) the OGD/R-mediated upregulation of *Casp3*. *Casp3* levels are largely regulated by the let-7-5p miR family^{39,40}, and hWJ-MSC-derived EVs contained members of the let-7-5p family, as measured by real-

Table 1. Mature miR Content of hWJ-MSC-derived EVs and Their Proapoptotic Target Genes with Target Scores ≥ 70 (miRDB.org).

Mature miR	Target Gene
let-7b-5p	<i>Casp3</i>
let-7c-5p	<i>Casp3</i>
let-7d-5p	<i>Casp3</i>
let-7e-5p	<i>Casp3</i>
let-7i-5p	<i>Casp3</i>
miR-9-3p	<i>BNIP3L</i>
miR-20a-5p	<i>Casp8</i>
miR-24-3p	<i>BOK; BNIP3L; BCL2L11</i>
miR-26b-5p	<i>CRADD</i>
miR-28-5p	<i>Casp2</i>
miR-29a-3p	<i>HRK; BMF</i>
miR-29b-3p	<i>HRK; BMF</i>
miR-29c-3p	<i>HRK; BMF</i>
miR-30d-5p	<i>BNIP3L; BCL10</i>
miR-34a-5p	<i>Casp2; BCL2L13</i>
miR-92a-3p	<i>BCL2L11</i>
miR-93-5p	<i>Casp8</i>
miR-98-5p	<i>Casp3</i>
miR-106b-5p	<i>Casp8</i>
miR-125-5p	<i>BCL2L14; BMF</i>
miR-133b	<i>BNIP3L</i>
miR-138-5p	<i>Casp7; BNIP3L</i>
miR-181a-5p	<i>BCLAF1</i>
miR-181d-5p	<i>BCLAF1</i>
miR-203a-3p	<i>BCL2L11</i>
miR-298	<i>BCL2L1</i>
miR-320a	<i>BNIP3</i>
miR-342-3p	<i>Casp2</i>
miR-409-3p	<i>BNIP3L</i>
miR-432-5p	<i>Casp14</i>

Abbreviations: EVs, extracellular vesicles; hWJ-MSCs, human Wharton's jelly mesenchymal stem cells; miR, microRNA; Casp3, caspase 3; BNIP3L, BCL2 interacting protein 3 like; Casp8, caspase 8; BOK, BOK, BCL2 family apoptosis regulator; BCL2L11, BCL2 like 11; CRADD, CASP2 and RIPK1 domain containing adaptor with death domain; Casp2, caspase 2; HRK, harakiri, BCL2 interacting protein; BMF, Bcl2 modifying factor; BCL10, B-cell CLL/lymphoma 10; BCL2L13, BCL2 like 13; Casp8, caspase 8; Casp3, caspase 3; BCL2L14, BCL2 like 14; Casp7, caspase 7; BCLAF1, BCL2 associated transcription factor 1; BCL2L1, BCL2 like 1; BNIP3, BCL2 interacting protein 3; Casp14, caspase 14.

time PCR (Table 1). Thus, we next measured the levels of let-7a and let-7e in N2a cells after OGD/R with and without EVs. Six hours of OGD and 24 h of reoxygenation significantly decreased let-7a ($P = 0.032$) and let-7e ($P = 0.003$) expression in N2a cells relative to undamaged cells (Fig. 4D). Adding 1 $\mu\text{g}/\text{mL}$ (ca. 20 pg/cell) EVs 1 h before OGD/R significantly increased let-7e expression in N2a cells compared to damaged cells ($P = 0.010$). However, let-7e levels did not change when 1 $\mu\text{g}/\text{mL}$ EVs were added 24 h before OGD/R induction relative to damaged cells. Let-7a expression was not significantly altered in N2a cells when 1 $\mu\text{g}/\text{mL}$ EVs were added 24 h or 1 h before the onset of OGD/R (Fig. 4D). No changes in let-7a and let-7e levels were detected after 48 h of reoxygenation (data not shown).

The significant decrease of let-7a in N2a cells subjected to 6 h OGD and 24 h reoxygenation was reversed by the

addition of 1 $\mu\text{g}/\text{mL}$ EVs directly after OGD (ca. 20 pg/cell; $P = 0.021$; Fig. 4E). Although 6 h OGD and 24 h of reoxygenation significantly declined let-7e levels in N2a cells ($P = 0.003$), treatment with EVs post-OGD did not increase let-7e expression levels to a significant degree (Fig. 4E). No alterations of let-7a and let-7e expression were measured after 48 h of reoxygenation (data not shown).

Discussion

We successfully isolated EVs derived from hWJ-MSCs by serial high-speed centrifugation and ultracentrifugation. Obtained EV preparations were derived from endosomes and were not contaminated by organelle-bearing apoptotic bodies, verified by the absent expression of the Golgi complex marker CM130 and the endoplasmic chaperone GRP94, their nanoscale size, and their morphology.

We showed that OGD/R-initiated apoptosis could be prevented and resolved by hWJ-MSC-derived EVs. The treatment of N2a cells with hWJ-MSC-derived EVs even post-OGD initiation rectified the apoptotic cascade.

We observed that hWJ-MSC-derived EVs interfere with the apoptotic cascade at the transcriptional level of *Casp3* and at the phosphorylation status of the pro-apoptotic Bcl2 protein family member BAD. By forming a pore in the mitochondrial outer membrane, the Bcl2 family regulates a key step in the initiation of the apoptotic pathway⁴¹. The proapoptotic activity of BAD is regulated by the phosphorylation of serines. In normal cells, BAD is phosphorylated and therefore inactive and sequestered into the cytoplasm. Non-p-BAD is active by forming heterodimers with the anti-apoptotic BCL-2 members BCL-2 and BCL-XL and, thus, initiating the apoptotic cascade. While the transcription of *Bad* was increased in N2a cells after OGD/R, the addition of hWJ-MSC-derived EVs before and after the OGD exposure of N2a cells, respectively, did not significantly prevent or resolve the elevated *Bad* gene expression, indicating that hWJ-MSC-derived EVs do not regulate the transcription of *Bad*. However, a higher sample number would be needed to test for significance. At the protein level, phosphorylation of BAD in N2a cells did not change after OGD/R, suggesting that OGD/R-mediated apoptosis in N2a cells is rather triggered by the increased transcription of *Bad*—and probably by translation into unphosphorylated BAD—than by the desphosphorylation of p-BAD. hWJ-MSC-derived EVs, added before or after OGD initiation, tended to increase the phosphorylation of BAD in N2a cells, providing evidence that hWJ-MSC-derived EVs interfere with apoptosis, at least in part, by increasing the proportion of the inactive p-BAD relative to the proapoptotic unphosphorylated BAD. However, to complete this hypothesis, the p-BADSer112/BAD ratio should be determined.

The sequential activation of caspases, a cysteine protease family, is pivotal in the execution stage of apoptosis and is required for neurodegeneration in neonatal HI brain damage⁴⁻⁶. In living cells, caspases are present as inactive

proenzymes. After the initiation of the apoptotic cascade, caspases are cleaved into 2 subunits, which for their part dimerize and build up the active enzyme⁴². The addition of hWJ-MSC-derived EVs to N2a cells both prior to and post-OGD exposure prevented and resolved the OGD/R-triggered transcription of *Casp3*, emphasizing their neuroprotective and neuroregenerative capacity. As the let-7-5p miR family is known to regulate *Casp3*^{39,40} and we observed that hWJ-MSC-derived EVs contained several members of the let-7-5p miR family, along with numerous other miR targeting proapoptotic genes, we hypothesized that EV-derived let-7-5p miR regulated *Casp3* expression in N2a cells. Indeed, we showed that hWJ-MSC-derived EVs transferred their RNA into N2a cells. Furthermore, the expressions of *Casp3*, and let-7a and let-7e, respectively, were reciprocal, providing evidence that hWJ-MSC-derived EVs disturbed the OGD/R-mediated increase of *Casp3* by their let-7-5p miR cargo. However, the significant differences in let-7a and let-7e were measured after 24 h of reoxygenation, whereas changes in *Casp3* were significant only after 48 h of reoxygenation, indicating that the let-7-5p miR family negatively regulates *Casp3* expression by progressive mRNA degradation. The transfer of functional miR from MSC exosomes into target cells has also been demonstrated lately in several animal models, such as optic nerve crush, myocardial infarction, and right MCAO^{22,43,44}.

In conclusion, our present study suggests that hWJ-MSC-derived EVs protect against HI-induced neuronal cell death, which is of interest in regard to a previous report documenting a protective effect of EVs derived from human umbilical cord tissue-derived MSCs against H₂O₂-triggered cell death in rat myoblasts and kidney cells and human liver cells⁴⁵. Not only the neuroprotective capacity, but especially the neuroregenerative potential in HI-mediated damage by hWJ-MSC-derived EVs bears good prospects for their future clinical application in perinatal brain injury. However, before considering clinical practice, further investigation will be required on the molecular mechanisms of neuroprotection and neuroregeneration mediated by hWJ-MSC-derived EVs. To complete our understanding of hWJ-MSC-derived EVs as a therapeutic agent, the neuroprotective and neuroregenerative potential of hWJ-MSC-derived EVs has to be confirmed in a preclinical animal model of perinatal HI brain damage.

Authors' Note

Marianne S. Joerger-Messerli and Byron Oppliger contributed equally to this work.

Acknowledgments

Transmission electron microscopy was performed by Beat Haenni on equipment supported by the Microscopy Imaging Center (MIC), University of Bern, Switzerland. Confocal microscopy acquisition and analysis were performed by Carlos Wotzkow and with the support of the Live Cell Imaging Core Facility of the

Department of BioMedical Research coordinated by the MIC, University of Bern, Switzerland.

Ethical Approval

This study was approved by our institutional review board.

Statement of Human and Animal Rights

This article does not contain any studies with human or animal subjects.

Statement of Informed Consent

There are no human subjects in this article. Informed written consent was obtained for the donation of umbilical cords.

Declaration of Conflicting Interests

The author(s) declared no potential conflicts of interest with respect to the research, authorship, and/or publication of this article.

Funding

The author(s) disclosed receipt of the following financial support for the research, authorship, and/or publication of this article: This study was supported by the R'Equip grant from the Swiss National Science Foundation Nr. 316030_14500 and in part by CryoSave Switzerland and Gottfried and Julia Bangerter-Rhyner Foundation.

References

1. Rocha-Ferreira E, Hristova M. Plasticity in the neonatal brain following hypoxic-ischaemic injury. *Neural Plast.* 2016;2016:4901014.
2. Johnston MV, Trescher WH, Ishida A, Nakajima W. Neurobiology of hypoxic-ischemic injury in the developing brain. *Pediatric Res.* 2001;49(6):735–741.
3. Vannucci SJ, Hagberg H. Hypoxia-ischemia in the immature brain. *J Exp Biol.* 2004;207(Pt 18):3149–3154.
4. Zhu C, Wang X, Xu F, Bahr BA, Shibata M, Uchiyama Y, Hagberg H, Blomgren K. The influence of age on apoptotic and other mechanisms of cell death after cerebral hypoxia-ischemia. *Cell Death Differ.* 2005;12(2):162–176.
5. Du Y, Bales KR, Dodel RC, Hamilton-Byrd E, Horn JW, Czilli DL, Simmons LK, Ni B, Paul SM. Activation of a caspase 3-related cysteine protease is required for glutamate-mediated apoptosis of cultured cerebellar granule neurons. *Proc Natl Acad Sci U S A.* 1997;94(21):11657–11662.
6. Schulz JB, Weller M, Moskowitz MA. Caspases as treatment targets in stroke and neurodegenerative diseases. *Ann Neurol.* 1999;45(4):421–429.
7. Barkhuizen M, van den Hove DL, Vles JS, Steinbusch HW, Kramer BW, Gavilanes AW. 25 years of research on global asphyxia in the immature rat brain. *Neurosci Biobehav Rev.* 2017;75:166–182.
8. Azzopardi D, Strohm B, Marlow N, Brocklehurst P, Deierl A, Eddama O, Goodwin J, Halliday HL, Juszczak E, Kapellou O, et al. Effects of hypothermia for perinatal asphyxia on childhood outcomes. *N Engl J Med.* 2014;371(2):140–149.
9. Jacobs SE, Berg M, Hunt R, Tarnow-Mordi WO, Inder TE, Davis PG. Cooling for newborns with hypoxic ischaemic

- encephalopathy. *Cochrane Database Syst Rev.* 2013;(1): CD003311.
10. Oppliger B, Joerger-Messerli M, Mueller M, Reinhart U, Schneider P, Surbek DV, Schoeberlein A. Intranasal delivery of umbilical cord-derived mesenchymal stem cells preserves myelination in perinatal brain damage. *Stem Cells Dev.* 2016; 25(16):1234–1242.
 11. Sizonenko SV, Sirimanne E, Mayall Y, Gluckman PD, Inder T, Williams C. Selective cortical alteration after hypoxic-ischemic injury in the very immature rat brain. *Pediatric Res.* 2003;54(2):263–269.
 12. Stadlin A, James A, Fiscus R, Wong YF, Rogers M, Haines C. Development of a postnatal 3-day-old rat model of mild hypoxic-ischemic brain injury. *Brain Res.* 2003;993(1-2):101–110.
 13. Parr AM, Tator CH, Keating A. Bone marrow-derived mesenchymal stromal cells for the repair of central nervous system injury. *Bone Marrow Transplant.* 2007;40(7):609–619.
 14. Burns TC, Verfaillie CM, Low WC. Stem cells for ischemic brain injury: a critical review. *J Comp Neurol.* 2009;515(1):125–144.
 15. Katsuda T, Kosaka N, Takeshita F, Ochiya T. The therapeutic potential of mesenchymal stem cell-derived extracellular vesicles. *Proteomics.* 2013;13(10-11):1637–1653.
 16. Pan BT, Johnstone RM. Fate of the transferrin receptor during maturation of sheep reticulocytes in vitro: selective externalization of the receptor. *Cell.* 1983;33(3):967–978.
 17. Harding C, Heuser J, Stahl P. Endocytosis and intracellular processing of transferrin and colloidal gold-transferrin in rat reticulocytes: demonstration of a pathway for receptor shedding. *Eur J Cell Biol.* 1984;35(2):256–263.
 18. Raposo G, Nijman HW, Stoorvogel W, Liejendekker R, Harding CV, Melief CJ, Geuze HJ. B lymphocytes secrete antigen-presenting vesicles. *J Exp Med.* 1996;183(3):1161–1172.
 19. EL Andaloussi S, Mager I, Breakefield XO, Wood MJ. Extracellular vesicles: biology and emerging therapeutic opportunities. *Nat Rev Drug Discov.* 2013;12(5):347–357.
 20. Raposo G, Stoorvogel W. Extracellular vesicles: exosomes, microvesicles, and friends. *J Cell Biol.* 2013;200(4):373–383.
 21. Zhuang X, Xiang X, Grizzle W, Sun D, Zhang S, Axtell RC, Ju S, Mu J, Zhang L, Steinman L, et al. Treatment of brain inflammatory diseases by delivering exosome encapsulated anti-inflammatory drugs from the nasal region to the brain. *Mol Ther.* 2011;19(10):1769–1779.
 22. Xin H, Li Y, Buller B, Katakowski M, Zhang Y, Wang X, Shang X, Zhang ZG, Chopp M. Exosome-mediated transfer of miR-133b from multipotent mesenchymal stromal cells to neural cells contributes to neurite outgrowth. *Stem Cells.* 2012; 30(7):1556–1564.
 23. Doeppner TR, Herz J, Gorgens A, Schlechter J, Ludwig AK, Radtke S, de Miroshedji K, Horn PA, Giebel B, Hermann DM. Extracellular vesicles improve post-stroke neuroregeneration and prevent posts ischemic immunosuppression. *Stem Cells Transl Med.* 2015;4(10):1131–1143.
 24. Hu B, Chen S, Zou M, He Z, Shao S, Liu B. Effect of extracellular vesicles on neural functional recovery and immunologic suppression after rat cerebral apoplexy. *Cell Physiol Biochem.* 2016;40(1-2):155–162.
 25. Ophelders DR, Wolfs TG, Jellema RK, Zwanenburg A, Andriessen P, Delhaas T, Ludwig AK, Radtke S, Peters V, Janssen L, et al. Mesenchymal stromal cell-derived extracellular vesicles protect the fetal brain after hypoxia-ischemia. *Stem Cells Transl Med.* 2016;5(6):754–763.
 26. Burke J, Kolhe R, Hunter M, Isales C, Hamrick M, Fulzele S. Stem cell-derived exosomes: a potential alternative therapeutic agent in orthopaedics. *Stem Cells Int.* 2016;2016:5802529.
 27. Gneocchi M, Danieli P, Malpasso G, Ciuffreda MC. Paracrine mechanisms of mesenchymal stem cells in tissue repair. *Methods Mol Biol.* 2016;1416:123–146.
 28. Vishnubhatla I, Corteling R, Stevanato L, Hicks C, Sinden J. The development of stem cell-derived exosomes as a cell-free regenerative medicine. *J Circ Biomarkers.* 2014;3(2):1–14.
 29. He L, Hannon GJ. MicroRNAs: small RNAs with a big role in gene regulation. *Nat Rev Genet.* 2004;5(7):522–531.
 30. Katakowski M, Buller B, Zheng X, Lu Y, Rogers T, Osobamiro O, Shu W, Jiang F, Chopp M. Exosomes from marrow stromal cells expressing miR-146b inhibit glioma growth. *Cancer Lett.* 2013;335(1):201–204.
 31. Lee JK, Park SR, Jung BK, Jeon YK, Lee YS, Kim MK, Kim YG, Jang JY, Kim CW. Exosomes derived from mesenchymal stem cells suppress angiogenesis by down-regulating VEGF expression in breast cancer cells. *PLoS One.* 2013;8(12):e84256.
 32. Messerli M, Wagner A, Sager R, Mueller M, Baumann M, Surbek DV, Schoeberlein A. Stem cells from umbilical cord Wharton’s jelly from preterm birth have neuroglial differentiation potential. *Reprod Sci.* 2013;20(12):1455–1464.
 33. Théry C, Amigorena S, Raposo G, Clayton A. Isolation and characterization of exosomes from cell culture supernatants and biological fluids. *Curr Protoc Cell Biol.* 2006;Chapter 3: Unit 3.22.
 34. Mueller M, Schoeberlein A, Zhou J, Joerger-Messerli M, Oppliger B, Reinhart U, Bordey A, Surbek D, Barnea ER, Huang Y, et al. Preimplantation Factor bolsters neuroprotection via modulating Protein Kinase A and Protein Kinase C signaling. *Cell Death Differ.* 2015;22(12):2078–2086.
 35. Blomgren K, Zhu C, Wang X, Karlsson JO, Leverin AL, Bahr BA, Mallard C, Hagberg H. Synergistic activation of caspase-3 by m-calpain after neonatal hypoxia-ischemia: a mechanism of “pathological apoptosis”? *J Biol Chem.* 2001;276(13): 10191–10198.
 36. Cheng Y, Deshmukh M, D’Costa A, Demaro JA, Gidday JM, Shah A, Sun Y, Jacquin MF, Johnson EM, Holtzman DM. Caspase inhibitor affords neuroprotection with delayed administration in a rat model of neonatal hypoxic-ischemic brain injury. *J Clin Invest.* 1998;101(9):1992–1999.
 37. Hu BR, Liu CL, Ouyang Y, Blomgren K, Siesjo BK. Involvement of caspase-3 in cell death after hypoxia-ischemia declines during brain maturation. *J Cereb Blood Flow Metab.* 2000; 20(9):1294–1300.
 38. Danial NN. BAD: undertaker by night, candyman by day. *Oncogene.* 2008;27(Suppl 1):S53–S70.
 39. Tsang WP, Kwok TT. Let-7a microRNA suppresses therapeutics-induced cancer cell death by targeting caspase-3. *Apoptosis.* 2008;13(10):1215–1222.

40. Peng G, Yuan Y, He Q, Wu W, Luo BY. MicroRNA let-7e regulates the expression of caspase-3 during apoptosis of PC12 cells following anoxia/reoxygenation injury. *Brain Res Bull.* 2011;86(3-4):272–276.
41. Shamas-Din A, Kale J, Leber B, Andrews DW. Mechanisms of action of Bcl-2 family proteins. *Cold Spring Harb Perspect Biol.* 2013;5(4):a008714.
42. Shi Y. Caspase activation: revisiting the induced proximity model. *Cell.* 2004;117(7):855–858.
43. Mead B, Tomarev S. Bone marrow-derived mesenchymal stem cells-derived exosomes promote survival of retinal ganglion cells through miRNA-dependent mechanisms. *Stem Cells Transl Med.* 2017;6(4):1273–1285.
44. Wang K, Jiang Z, Webster KA, Chen J, Hu H, Zhou Y, Zhao J, Wang L, Wang Y, Zhong Z, et al. Enhanced cardioprotection by human endometrium mesenchymal stem cells driven by exosomal MicroRNA-21. *Stem Cells Transl Med.* 2017;6(1):209–222.
45. Zhang B, Shen L, Shi H, Pan Z, Wu L, Yan Y, Zhang X, Mao F, Qian H, Xu W. Exosomes from human umbilical cord mesenchymal stem cells: identification, purification, and biological characteristics. *Stem Cells Int.* 2016;2016:1929536.